ANNUAL REVIEWS

Annual Review of Fluid Mechanics

Double-Diffusive Convection at Low Prandtl Number

Pascale Garaud

Department of Applied Mathematics and Statistics, Baskin School of Engineering, University of California, Santa Cruz, California 95064; email: pgaraud@ucsc.edu

Annu. Rev. Fluid Mech. 2018. 50:275–98

First published as a Review in Advance on October 6, 2017

The *Annual Review of Fluid Mechanics* is online at fluid.annualreviews.org

https://doi.org/10.1146/annurev-fluid-122316-045234

Keywords

convection, double-diffusive convection, direct numerical simulations, astrophysical fluid dynamics, thermohaline convection, semiconvection

Abstract

This work reviews present knowledge of double-diffusive convection at low Prandtl number obtained using direct numerical simulations, in both the fingering regime and the oscillatory regime. Particular emphasis is given to modeling the induced turbulent mixing and its impact in various astrophysical applications. The nonlinear saturation of fingering convection at low Prandtl number usually drives small-scale turbulent motions whose transport properties can be predicted reasonably accurately using a simple semi-analytical model. In some instances, large-scale internal gravity waves can be excited by a collective instability and eventually cause layering. The nonlinear saturation of oscillatory double-diffusive convection exhibits much more complex behavior. Weakly stratified systems always spontaneously transition into layered convection associated with very efficient mixing. More strongly stratified systems remain dominated by weak wave turbulence unless they are initialized into a layered state. The effects of rotation, shear, lateral gradients, and magnetic fields are briefly discussed.

1. INTRODUCTION

Double-diffusive convection loosely refers to the nonlinear outcome of a class of multicomponent buoyancy-driven instabilities taking place in dynamically stable fluids when the density depends on two different components that diffuse at different rates. Dynamical stability in this context requires that the density (prior to the development of the instability) be horizontally invariant and increase in the direction of gravity, thus ruling out standard overturning convection, baroclinic instabilities, and gravity currents. The unequal diffusivities of the two components become a necessary condition for instability.

Double-diffusive convection can take different forms depending on the sign of the mean gradients of each individual component of the density. This review focuses on two cases: (*a*) fingering convection, which occurs when the slowly diffusing component is unstably stratified and the rapidly diffusing one is stable, and (*b*) oscillatory double-diffusive convection (ODDC), which occurs when the slowly diffusing component is stably stratified and the rapidly diffusing one is unstable. For simplicity, in this review, I refer to the rapidly diffusing component as temperature and to the slowly diffusing one as composition, even though any results presented would apply equally well to isothermal cases where density depends on the concentration of two distinct chemicals instead.

The best-known examples of double-diffusive convection in geophysics take place in the Earth's oceans, where the density of water depends both on temperature and on salinity. Fingering instabilities and oscillatory double-diffusive instabilities were in fact first discovered in physical oceanography (Stern 1960) and have been studied in depth in this context (Turner 1974, 1985; Radko 2013). Other examples of naturally occurring geophysical double-diffusive convection have been found in geothermally active lakes and inland seas (Wüest et al. 2012), in the context of mushy layers (e.g., Worster 1997), or multicomponent flows through porous media (Nield 1968).

Despite their differences, all these geophysical examples share a common feature, namely, that the Prandtl number Pr (the ratio of the kinematic viscosity ν to the thermal diffusivity κ_T—more generally, the ratio of ν to the diffusivity of the rapidly diffusing component) is of order one or larger: Pr is of $\mathcal{O}(1)$ for standard gases, $\mathcal{O}(10)$ for water, and exceeds 10^4 for magmas. As such, most investigations of double-diffusive convection to date have focused on the high-Pr regime.

By contrast, the limit where $\mathrm{Pr} \ll 1$ or even $\mathrm{Pr} \to 0$ has received much less attention. It is nevertheless relevant for liquid metals where $\mathrm{Pr} \sim 10^{-3}$–10^{-1} (with application to metallurgy and planetary interiors) and in the hot dense plasmas found in stellar interiors where $\mathrm{Pr} \sim 10^{-9}$–10^{-5}. In both cases, Pr is small because κ_T is strongly enhanced relative to ν by electron conduction in liquid metals and by photon transport in stellar interiors. The ratio τ of the compositional to thermal diffusivities is also small for the same reasons. Unfortunately, physical experimentation in the low-Pr parameter regime is either extremely difficult or effectively impossible, which is why any progress in this area had to wait until three-dimensional (3D) direct numerical simulations (DNSs) of double-diffusive convection became routinely possible. In the past 10 years, however, advances in supercomputing have revolutionized the field. By solving the exact governing equations of fluid dynamics and by giving access to the entire spatiotemporal structure of each field (velocity, temperature, and composition), DNSs have become a most powerful tool for numerical experimentation.

I now review very briefly some of the pertinent properties of fingering convection and ODDC at high Pr before describing recent progress in studying double-diffusive convection at low Pr using DNSs.

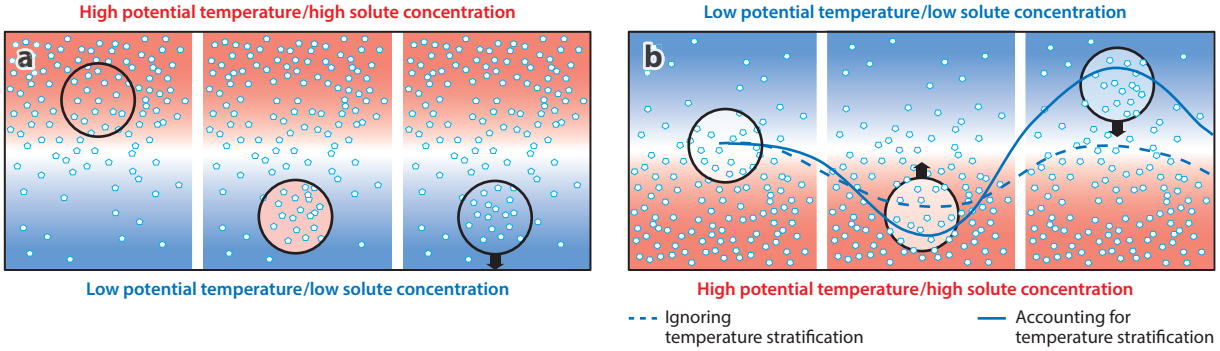

Figure 1

Illustration of (*a*) the fingering instability and (*b*) the oscillatory double-diffusive instability.

1.1. Fingering Convection

The driving mechanism for the fingering instability is illustrated in **Figure 1*a***, assuming that increasing the solute concentration C also increases density. When a small parcel of fluid from the warm and high-C upper layers is displaced downward, its temperature rapidly equilibrates with its surroundings via diffusion, but its concentration does not. Cooling gradually causes the density within the parcel to increase until it exceeds that of the local background, at which point the parcel proceeds to sink further. An optimal parcel size is required for this process to occur: If it is too large, thermal diffusion does not have time to take place before the buoyancy force pushes the parcel back up; if it is too small, viscosity suppresses the instability. Across most of parameter space (i.e., high and low Pr), typical fingering structures have width of order (Stern 1960)

$$d = \left(\frac{\kappa_T \nu}{N^2}\right)^{1/4}, \qquad 1.$$

where N is the local buoyancy frequency associated with the temperature field only. The fingering-unstable region of parameter space is relatively large, especially when the diffusivity ratio $\tau = \kappa_C/\kappa_T$ (where κ_C is the compositional diffusivity) is low (see Section 2).

After saturation, fingering convection usually takes the form of thin, more or less laminar tubes of high-C material flowing down and low-C fluid flowing up. However, one of the more remarkable high-Pr properties of fingering convection is its propensity to excite secondary instabilities on scales much larger than the basic finger scale. These include the development of large-scale internal gravity waves (Stern 1969) and of thermocompositional staircases (Stern & Turner 1969), i.e., stacks of well-mixed convective layers separated by stably stratified fingering interfaces. The staircases are robust when they form and can be horizontally coherent over huge distances. They are commonly observed in laboratory experiments (Krishnamurti 2003), as well as in the ocean (Tait & Howe 1968, 1971). Their presence can increase the turbulent heat and compositional fluxes across the fingering region by several orders of magnitude above that of small-scale fingering convection (Schmitt et al. 2005).

1.2. Oscillatory Double-Diffusive Convection

The basic instability associated with ODDC takes the form of an unstable gravity wave (Walin 1964). In the absence of a background temperature gradient, the compositional gradient alone is stabilizing and any initial perturbation would generate a stable oscillation in the form of internal

gravity waves (see **Figure 1*b***). The destabilizing temperature gradient, however, causes a sufficiently small oscillating parcel of fluid to cool down or warm up via diffusion at the peaks and troughs of its motion, respectively. Under the right conditions, this can gradually enhance the amplitude of the oscillation. The size of the parcel must be optimally chosen for the instability to proceed. It has been shown to be $\mathcal{O}(d)$, as in the fingering case (Walin 1964, Kato 1966, Baines & Gill 1969).

In contrast with the fingering instability, however, the region of parameter space that is linearly unstable to ODDC (in the manner described above) at high Pr is too small to be of any practical relevance (see Section 2) because viscosity has a strong damping effect on the necessarily small-scale oscillations. Despite this, thermohaline layering associated with ODDC is nearly ubiquitously observed in the Arctic (Timmermans et al. 2008) and in geothermally active lakes (Wüest et al. 2012) even when all the system parameters lie well outside the linearly unstable range, suggesting that other destabilizing mechanisms may be at play (e.g., see Veronis 1965, Huppert & Moore 1976, Proctor 1981, Radko 2016). These so-called diffusive staircases have very stable interfaces that are almost entirely quiescent. As in the fingering case, they are also extremely robust and can be coherent over huge distances. The rate of heat and compositional transport across the staircase is typically limited by the diffusive fluxes across each interface and, as such, is much smaller than for fingering interfaces but not negligible since the interfaces are very thin.

As I demonstrate in this review, the dynamics of double-diffusive convection (fingering convection and ODDC) at low Pr are sometimes similar to, and sometimes notably different from, those arising at high Pr. The crucial difference between the two regimes can be understood by noting that whereas viscous diffusion is significant on the scale of d (i.e., the finger scale or the basic ODDC scale) when $\mathrm{Pr} \gg 1$, it is usually negligible when $\mathrm{Pr} \ll 1$. As such, inertial terms tend to dominate the system dynamics at low Pr, with all the possible consequences that this may imply. In what follows, I therefore review very recent progress in our understanding of double-diffusive convection in the low-Pr limit (i.e., roughly speaking, from $\mathrm{Pr} \leq 0.3$ down to $\mathrm{Pr} \to 0$). The linear stability analysis of Section 2 is included by way of introducing the model setup as well as for completeness. Section 3 provides a synthetic summary of recent works on fingering convection at low Pr, whereas Section 4 describes parallel progress on the study of low-Pr ODDC. I then present various applications of these findings to planetary science and stellar astrophysics in Section 5 and very briefly discuss in Section 6 the effects of additional physical processes such as rotation, shear, magnetic fields, lateral gradients, and finite-amplitude instabilities.

2. LINEAR STABILITY OF THERMOCOMPOSITIONAL DOUBLE-DIFFUSIVE CONVECTION

A commonly adopted model setup for the study of double-diffusive convection with application to geophysics or astrophysics [where the turbulent scale $\mathcal{O}(d)$ is expected to be orders of magnitude smaller than the size of the unstable region] is one that minimizes the effect of boundaries as much as possible by considering triply periodic perturbations to linearly varying temperature and composition profiles (e.g., Baines & Gill 1969, Shen 1995, Radko 2013). Since the root mean square velocity of the turbulent flow is also usually very small compared to the local sound speed, it is customary to use the Boussinesq approximation for weakly compressible gases (Spiegel & Veronis 1960), which can be used to study double-diffusive convection not only in liquids but also in the Earth's atmosphere, as well as in stellar and planetary interiors. Consistent with this approximation is the use of a linearized equation of state, where temperature and composition perturbations, denoted by T and C, respectively, are linearly related to the density perturbations ρ.

The governing equations for double-diffusive convection are

$$\rho_{\mathrm{m}}\left(\frac{\partial \mathbf{u}}{\partial t}+\mathbf{u}\cdot\nabla\mathbf{u}\right)=-\nabla p-\rho g\mathbf{e}_z+\rho_{\mathrm{m}}\nu\nabla^2\mathbf{u}, \qquad 2.$$

$$\frac{\rho}{\rho_{\mathrm{m}}}=-\alpha T+\beta C, \qquad \nabla\cdot\mathbf{u}=0, \qquad 3.$$

$$\frac{\partial T}{\partial t}+\mathbf{u}\cdot\nabla T+\left(\frac{\mathrm{d}T_0}{\mathrm{d}z}-\frac{\mathrm{d}T_{\mathrm{ad}}}{\mathrm{d}z}\right)w=\kappa_T\nabla^2 T, \qquad 4.$$

$$\frac{\partial C}{\partial t}+\mathbf{u}\cdot\nabla C+\frac{\mathrm{d}C_0}{\mathrm{d}z}w=\kappa_C\nabla^2 C, \qquad 5.$$

where ρ_{m} is the mean density of the region considered, $\mathbf{u}=(u,v,w)$ is the velocity field, p is the pressure perturbation, g is the gravitational acceleration, α and β are related to derivatives of the equation of state, $\mathrm{d}T_0/\mathrm{d}z$ and $\mathrm{d}C_0/\mathrm{d}z$ are the assumed background temperature and composition gradients, respectively, and $\mathrm{d}T_{\mathrm{ad}}/\mathrm{d}z=-g/c_{\mathrm{p}}$ is the adiabatic temperature gradient (and c_{p} is the specific heat at constant pressure). Assuming that the vertical extent of the region considered is small, we simplify the problem by taking ρ_{m}, g, α, β, $\mathrm{d}T_0/\mathrm{d}z$, $\mathrm{d}C_0/\mathrm{d}z$, $\mathrm{d}T_{\mathrm{ad}}/\mathrm{d}z$, and all the diffusivities to be constant.

An appropriate choice of nondimensionalization is one where d is used as the unit length, d^2/κ_T is used as the unit of time, $d|\mathrm{d}T_0/\mathrm{d}z-\mathrm{d}T_{\mathrm{ad}}/\mathrm{d}z|$ is the unit temperature, and $(\alpha/\beta)d|\mathrm{d}T_0/\mathrm{d}z-\mathrm{d}T_{\mathrm{ad}}/\mathrm{d}z|$ is the unit composition (e.g., Radko 2013). The nondimensional governing equations are then

$$\frac{1}{\mathrm{Pr}}\left(\frac{\partial \mathbf{u}}{\partial t}+\mathbf{u}\cdot\nabla\mathbf{u}\right)=-\nabla p+(T-C)\mathbf{e}_z+\nabla^2\mathbf{u}, \qquad \nabla\cdot\mathbf{u}=0,$$

$$\frac{\partial T}{\partial t}+\mathbf{u}\cdot\nabla T\pm w=\nabla^2 T, \qquad \frac{\partial C}{\partial t}+\mathbf{u}\cdot\nabla C\pm\frac{w}{R_0}=\tau\nabla^2 C, \qquad 6.$$

where all quantities are now implicitly nondimensional. The $\pm$ signs in the temperature and composition equations correspond to the signs of $\mathrm{d}T_0/\mathrm{d}z-\mathrm{d}T_{\mathrm{ad}}/\mathrm{d}z$ and $\mathrm{d}C_0/\mathrm{d}z$, respectively, and are therefore all that differentiate the fingering convection equations (+ case) from the ODDC equations (− case). We see that three model parameters

$$\mathrm{Pr}=\frac{\nu}{\kappa_T}, \quad \tau=\frac{\kappa_C}{\kappa_T}, \quad \text{and} \quad R_0=\frac{\alpha\left|\frac{\mathrm{d}T_0}{\mathrm{d}z}-\frac{\mathrm{d}T_{\mathrm{ad}}}{\mathrm{d}z}\right|}{\beta\left|\frac{\mathrm{d}C_0}{\mathrm{d}z}\right|} \qquad 7.$$

now explicitly appear. The density ratio R_0 is a measure of the effective stratification of the system, with $R_0=1$ being neutrally stratified with respect to standard overturning convection: $\mathrm{d}\rho_0/\mathrm{d}z=-\alpha(\mathrm{d}T_0/\mathrm{d}z-\mathrm{d}T_{\mathrm{ad}}/\mathrm{d}z)+\beta\,\mathrm{d}C_0/\mathrm{d}z=0$ when $R_0=1$.

The linear stability of the system of Equation 6 was studied by Baines & Gill (1969). In a periodic domain, normal modes of the instability are of the form $\exp(ilx+imy+ikz+\lambda t)$, where all quantities are now nondimensional. The growth rate λ satisfies the cubic equation $\lambda^3+a_2\lambda^2+a_1\lambda+a_0=0$, where

$$a_2=(1+\mathrm{Pr}+\tau)|\mathbf{k}|^2,$$

$$a_1=(\tau+\mathrm{Pr}+\tau\mathrm{Pr})|\mathbf{k}|^4\pm\mathrm{Pr}\frac{L^2}{|\mathbf{k}|^2}\left(1-R_0^{-1}\right), \qquad 8.$$

$$a_0=\tau\mathrm{Pr}|\mathbf{k}|^6\pm\mathrm{Pr}L^2\left(\tau-R_0^{-1}\right),$$

where $\mathbf{k}=(l,m,k)$ is the total nondimensional wave vector, and $L=\sqrt{l^2+m^2}$ is the corresponding horizontal wave number. The $\pm$ signs in Equation 8 refer to fingering convection (+) and

ODCC (−), as in Equation 6. The fastest-growing modes are always vertically invariant (Radko 2013). In addition, (*a*) the fingering system is double-diffusively unstable provided $1 < R_0 < \tau^{-1}$, with $R_0 > \tau^{-1}$ being linearly stable, and (*b*) the ODDC system is double-diffusively unstable provided $1 < R_0^{-1} < \frac{\mathrm{Pr}+1}{\mathrm{Pr}+\tau}$, with $R_0^{-1} > \frac{\mathrm{Pr}+1}{\mathrm{Pr}+\tau}$ being linearly stable. This immediately reveals one of the most remarkable properties of the low Pr limit, namely, the dramatic increase in the range of inverse density ratios that are linearly unstable to ODDC, from a maximum value of order 1.1 for water ($\mathrm{Pr} \simeq 7, \tau \simeq 0.01$) to $\mathcal{O}(\mathrm{Pr}^{-1})$ when $\mathrm{Pr} \sim \tau \ll 1$.

In both cases, the nondimensional horizontal wave number of the fastest-growing mode is typically of order 1/2 across most of the instability range, except when the density ratio approaches marginal stability, in which case it drops to zero. Dimensionally, this implies that the width of the fastest-growing eigenmode is $\mathcal{O}(10d)$. Note that an interesting characteristic of these eigenmodes is that they are exact nonlinear solutions of the governing equations.

The growth rate $\lambda_{\max}$ and horizontal wave number $L_{\max}$ of the fastest-growing modes of instability usually need to be found numerically and have been computed by Schmitt (1983) for a wide range of Pr, τ, and R_0 for the fingering case. However, simple analytical approximations can be found in the limit where $\mathrm{Pr} \sim \tau \ll 1$, relevant for both astrophysical systems and liquid metals. Brown et al. (2013) studied the fingering case and showed that three different asymptotic limits exist depending on the reduced density ratio, $r_\mathrm{f} = (R_0 - 1)(\tau^{-1} - 1)^{-1}$, which maps the fingering-unstable region of parameter space onto the unit interval:

- If $r_\mathrm{f} \ll \mathrm{Pr}, \tau \ll 1$, then $\lambda_{\max} = \sqrt{\mathrm{Pr}} - \mathrm{Pr}\sqrt{1 + \mathrm{Sc}^{-1}} + \cdots$.
- If $\mathrm{Pr}, \tau \ll r_\mathrm{f} \ll 1$, then $\lambda_{\max} = \mathrm{Pr}\sqrt{\frac{\mathrm{Sc}^{-1}}{r_\mathrm{f}}} - \mathrm{Pr}\sqrt{1 + \mathrm{Sc}^{-1}} + \cdots$.
- If $r_\mathrm{f} \to 1$, then $\lambda_{\max} = 2\mathrm{PrSc}^{-1}\left[\frac{1-r_\mathrm{f}}{3} + \cdots\right]^{3/2}\left[1 - \frac{1+\mathrm{Sc}^{-1}}{3}(1 - r_\mathrm{f}) + \cdots\right]^{-1}$.

Here, $\mathrm{Sc}^{-1} = \tau/\mathrm{Pr} = \kappa_C/\nu$ is the inverse Schmidt number, assumed to be of order one. Mirouh et al. (2012) analyzed the ODDC case, where the appropriate reduced inverse density ratio is now $r_\mathrm{o} = (R_0^{-1} - 1)(\frac{\mathrm{Pr}+1}{\mathrm{Pr}+\tau} - 1)^{-1}$. In the limit of small Pr and small τ, with $\mathrm{Pr} \sim \tau$, they showed that the real part of the growth rate of the fastest-growing modes $\lambda_{R,\max}$ scales with Pr and that the horizontal wave number $L_{\max}$ remains of order one. Letting $\lambda_{R,\max} = \mathrm{Pr}\hat{\lambda}$, and $L_{\max} = \hat{L}$, they showed that $\hat{\lambda}$ and $\hat{L}$ asymptotically satisfy the following equation:

$$\hat{\lambda} = \frac{1 - r_\mathrm{o} - 3\hat{L}^4(1 + \mathrm{Sc}^{-1})}{4\hat{L}^2}, \qquad 9.$$

where

$$\hat{L}^4 = \frac{\sqrt{8r_\mathrm{o} + 1} - (2r_\mathrm{o} + 1)}{2(1 + \mathrm{Sc}^{-1})}.$$

To go beyond linear theory in the low-Pr parameter regime, numerical simulations are paramount. Thanks to the model setup adopted, the set of equations listed in Equation 6 can be efficiently evolved in time using high-performance pseudo-spectral algorithms (e.g., Traxler et al. 2011b). When $\tau \ll 1$, high resolution is crucial to resolve the thin compositional boundary layers that develop. For this reason, it may be tempting to work with 2D instead of 3D simulations (e.g., Denissenkov 2010, Moll et al. 2016). However, although this strategy works quite well at high Pr, inasmuch as the outcome of 2D and 3D simulations is often qualitatively similar (Stern et al. 2001), the same is not usually true at low Pr (Garaud & Brummell 2015; although see Moll et al. 2016). For this reason, I now limit the discussion about the nonlinear evolution of low-Pr fingering convection and ODDC to results obtained with 3D simulations only.

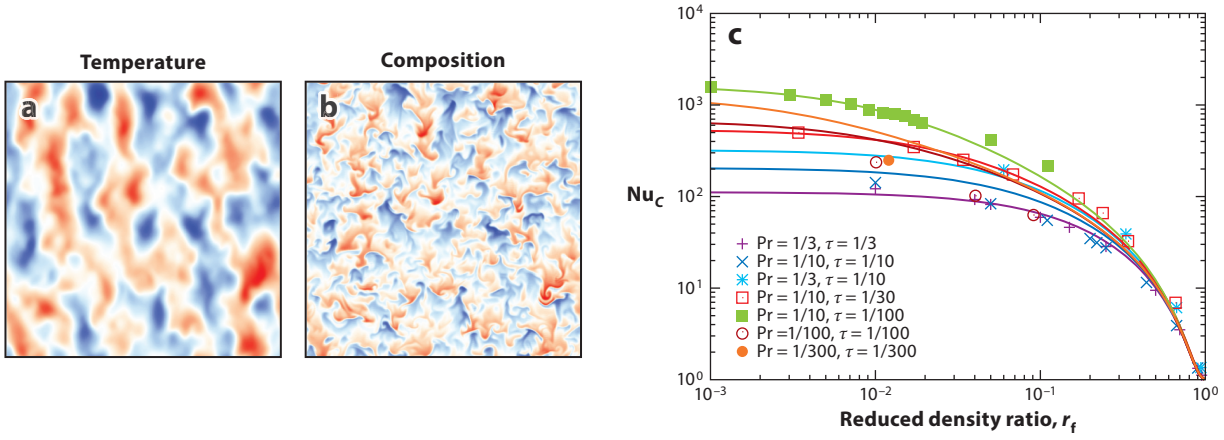

Figure 2

(*a*,*b*) Snapshots of the temperature and composition perturbations in a three-dimensional (3D) direct numerical simulation (DNS), where $\mathrm{Pr} = \tau = 0.01$ and $R_0 = 5$. (*c*) Measured and predicted compositional Nusselt number in all 3D DNSs available to date. Data presented are collected from Traxler et al. (2011a), Brown et al. (2013), and Radko & Smith (2012), as well as new data (P. Garaud, unpublished data). The solid lines are from the model of Brown et al. (2013), with $K = 7$.

3. NONLINEAR SATURATION OF FINGERING CONVECTION

3.1. Saturation of the Basic Instability

The first comprehensive 3D numerical experiments of low-Pr fingering convection were presented by Traxler et al. (2011a) and later extended by Radko & Smith (2012) and Brown et al. (2013). Numerical constraints limit achievable values of Pr and τ to 10^{-3} or greater. With the exception of one particular corner of parameter space discussed below (see Section 3.2.2), the fingering instability nearly always saturates into a statistically stationary, weakly turbulent state of homogeneous small-scale fingering convection (see **Figure 2*a*,*b***). The turbulent Reynolds numbers achieved after saturation are very moderate [at most a few hundreds for $\mathrm{Pr} \sim \tau \sim \mathcal{O}(10^{-1})$ and very low R_0] and decrease for lower Pr and τ or higher R_0. The typical horizontal size of the fingers is reasonably well approximated by the predictions from linear theory (Traxler et al. 2011a).

3.1.1. Numerical estimates of turbulent mixing after saturation. Given the selected model setup, the mixing efficiency of fingering convection can easily be measured using the thermal and compositional Nusselt numbers, defined here as

$$\mathrm{Nu}_T = 1 - \langle wT \rangle \text{ and } \mathrm{Nu}_C = 1 - \frac{R_0}{\tau}\langle wC \rangle, \qquad 10.$$

respectively, where the chevrons $\langle \cdot \rangle$ denote a volume and time average over the entire domain, once the system has reached a statistically stationary state. Nu_T and Nu_C can be interpreted as the ratio of the effective to microscopic diffusivities of potential temperature and composition, respectively. It can be easily shown that in this model setup, $\langle wT \rangle = -\langle |\nabla T|^2 \rangle$ and $R_0^{-1}\langle wC \rangle = -\tau \langle |\nabla C|^2 \rangle$, which implies that $\mathrm{Nu}_T \geq 1$ and $\mathrm{Nu}_C \geq 1$.

The numerical experiments of Traxler et al. (2011a) and Brown et al. (2013) show that Nu_T is always low, about 30 at most for Pr, $\tau \sim 0.3$, and $R_0 \to 1$, rapidly dropping to 1 as Pr and τ decrease or R_0 increases. This is consistent with the notion that significant thermal diffusion is

required for fingering to develop in the first place. On the other hand, Nu_C can be relatively large depending on the selected parameters (see **Figure 2*c***).

3.1.2. Semi-analytical models. Attempts to construct simple models for turbulent transport by fingering convection at low Pr date back to the 1970s and 1980s in the astrophysical literature. Notable works are those of Ulrich (1972) and Kippenhahn et al. (1980), who both proposed on dimensional grounds that $\mathrm{Nu}_C - 1 = K/R_0\tau$, where K is a nondimensional constant. These models are still used in most stellar evolution computations, even though they do not adequately capture the high-R_0 cutoff for linear stability. Denissenkov (2010) proposed an improved model where $\mathrm{Nu}_C - 1 = K\frac{1-R_0\tau^{-1}}{\tau(R_0-1)}$, which is consistent with the scalings of Ulrich (1972) and Kippenhahn et al. (1980) for intermediate R_0, but correctly accounts for the linear stability cutoff. It must, however, break down as $R_0 \to 1$.

More recently, Brown et al. (2013) studied the question of the saturation of the fingering instability at low Pr, attributing it to the development of secondary shear instabilities between upward and downward fingers. Their work closely follows that of Radko & Smith (2012) in the geophysical context, but makes a few additional simplifications that enable them to obtain simple semi-analytical estimates for Nu_T and Nu_C as functions of the model parameters Pr, τ, and R_0:

$$\mathrm{Nu}_C - 1 = \frac{K^2\lambda_{\max}^2}{\tau L_{\max}^2(\lambda_{\max} + \tau L_{\max}^2)} \text{ and } \mathrm{Nu}_T - 1 = \frac{K^2\lambda_{\max}^2}{L_{\max}^2(\lambda_{\max} + L_{\max}^2)}, \qquad 11.$$

where $\lambda_{\max}$ and $L_{\max}$ are the growth rates and horizontal wave numbers of the fastest-growing fingering modes (see Section 2), and K is a universal constant of order unity to be determined. By universal, it is implied that one should be able to explain all the available data using the same value of K. In this model, the turbulent flux ratio γ is

$$\gamma = \frac{\langle wT\rangle}{\langle wC\rangle} = \frac{R_0}{\tau}\frac{\mathrm{Nu}_T - 1}{\mathrm{Nu}_C - 1} = R_0\frac{\lambda_{\max} + \tau L_{\max}^2}{\lambda_{\max} + L_{\max}^2}, \qquad 12.$$

which is independent of K. This formula recovers exactly the prediction of Schmitt (1979). Brown et al. (2013) found that their model was in very good (although not perfect) agreement with all the data available for $K = 7$, for Pr and τ as low as 0.01, as long as $\tau \leq \mathrm{Pr}$ (see **Figure 2*c***). With more recently available data at lower Pr, this statement remains correct, although the model now tends to overestimate Nu_C somewhat systematically by a factor of $\sim$2 for the lowest available values of Pr and τ ($\sim$0.003). The model is also not quite as good when $\tau > \mathrm{Pr}$, suggesting that K may depend on the Schmidt number (although why this is the case remains to be determined). The $\tau > \mathrm{Pr}$ region of parameter space does not appear to be physically relevant, however.

3.2. Large-Scale Secondary Instabilities

As discussed in Section 1.1, fingering convection in geophysical systems is prone to the development of secondary large-scale instabilities leading to the excitation of internal gravity waves and to the formation of thermocompositional staircases. Since transport through staircases is significantly enhanced compared with that of homogeneous fingering convection, assessing whether secondary instabilities are also excited at low Pr is of paramount importance. These types of instabilities have been successfully studied in geophysics using mean-field theory. The terminology is loosely used here to describe models that study the evolution of structures on scales much larger than individual fingers via spatiotemporal averaging, using simple parameterizations to account for the effects of the small scales. I now briefly summarize this technique and then review the

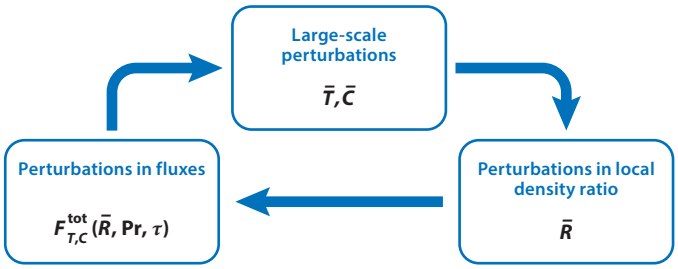

Figure 3

Illustration of positive feedback loops in mean-field instabilities. Large-scale perturbations in temperature and composition perturb the local density ratio, expressed nondimensionally as $\bar{R} = (1 + \partial\bar{T}/\partial z)(R_0^{-1} + \partial\bar{C}/\partial z)^{-1}$. This modulates Nu_T and γ and therefore also the total double-diffusive fluxes of temperature F_T^{tot} and composition F_C^{tot}. In a positive feedback loop, the divergence or convergence of the perturbed fluxes enhances the original perturbations.

results of its application to low-Pr fingering convection. Note that it is also directly applicable to ODDC.

3.2.1. Mean-field theory. The equations for the evolution of structures on large scales are

$$\frac{1}{\text{Pr}}\left(\frac{\partial\bar{\mathbf{u}}}{\partial t} + \bar{\mathbf{u}}\cdot\nabla\bar{\mathbf{u}} + \nabla\cdot\mathbf{R}\right) = -\nabla\bar{p} + (\bar{T} - \bar{C})\mathbf{e}_z + \nabla^2\bar{\mathbf{u}}, \qquad \nabla\cdot\bar{\mathbf{u}} = 0, \qquad 13.$$

$$\frac{\partial\bar{T}}{\partial t} + \bar{\mathbf{u}}\cdot\nabla\bar{T} + \nabla\cdot\mathbf{F}_T \pm \bar{w} = \nabla^2\bar{T}, \quad \frac{\partial\bar{C}}{\partial t} + \bar{\mathbf{u}}\cdot\nabla\bar{C} + \nabla\cdot\mathbf{F}_C \pm \frac{\bar{w}}{R_0} = \tau\nabla^2\bar{C}, \qquad 14.$$

where the overbar denotes a suitable average (e.g., an ensemble average or a horizontal average) and where

$$\mathbf{R} = \overline{\mathbf{u}\mathbf{u}}, \quad \mathbf{F}_T = \overline{\mathbf{u}T}, \text{ and } \mathbf{F}_C = \overline{\mathbf{u}C} \qquad 15.$$

are the specific Reynolds stress, the temperature flux, and the compositional flux, respectively. Within the context of geophysical fingering convection, various models have been proposed to express $\mathbf{R}$, $\mathbf{F}_T$, and $\mathbf{F}_C$ in terms of the large-scale fields $\bar{\mathbf{u}}$, $\bar{T}$, and $\bar{C}$ and their derivatives, and each of these models gives rise to a distinct set of nonlinear mean-field equations whose stability can then be studied using standard techniques. Despite their differences, mean-field models generally exhibit two main types of instabilities (in the absence of lateral gradients): (*a*) the collective instability (Stern 1969, Holyer 1981), which excites internal gravity waves, and (*b*) the γ-instability (Radko 2003), which causes vertical layering and ultimately the formation of thermocompositional staircases.

Traxler et al. (2011b) recently showed that the collective instability and the γ-instability can simply be viewed as different unstable modes of the same mean-field equations. Each mode corresponds to a particular positive feedback loop between large-scale perturbations and their effects on double-diffusive fluxes (see **Figure 3**). To construct their closure model, Traxler et al. (2011b) neglected the effects of Reynolds stresses. They assumed $\mathbf{F}_T = F_T\mathbf{e}_z = -(\text{Nu}_T - 1)\frac{\partial\bar{T}}{\partial z}\mathbf{e}_z$ and $\mathbf{F}_C = \gamma^{-1}\mathbf{F}_T$, where Nu_T and γ depend only on the fluid properties Pr, τ, and the local density ratio $\bar{R}$. The latter is given by $\bar{R} = \frac{1+\partial\bar{T}/\partial z}{R_0^{-1}+\partial\bar{C}/\partial z}$ and therefore varies when large-scale temperature and compositional perturbations are present. The functions $\text{Nu}_T(\bar{R})$ and $\gamma(\bar{R})$, for given Pr and τ, are assumed to be known.

Combining this closure model for $\mathbf{R}$, $\mathbf{F}_T$, and $\mathbf{F}_C$ with Equations 13 and 14 yields a set of mean-field equations that have a trivial solution: a state of homogeneous fingering convection in which $\bar{T} = \bar{C} = \bar{\mathbf{u}} = 0$, so that $\bar{R} = R_0$, $F_T = 1 - \text{Nu}_T(R_0)$, and $F_C = F_T/\gamma(R_0)$. Linearizing the mean-field equations around this state (assuming that the large-scale perturbations have small

amplitudes) yields a set of linear partial differential equations with constant coefficients. As for the basic instability, normal mode solutions exist and take the form $\bar{q} = \hat{\bar{q}} \exp(ilx + imy + ikz + \Lambda t)$, where Λ is the solution of a cubic equation. The coefficients of that cubic, which can be found in equation 2.13 of Traxler et al. (2011b), depend on the wave number $\mathbf{k}$, Pr, τ, and R_0 of course, but also on the mixing properties of the background state, namely, $\mathrm{Nu}_0 = \mathrm{Nu}_T(R_0)$ and $\gamma_0 = \gamma(R_0)$, as well as $A_1 = R_0 \frac{\mathrm{d}\gamma^{-1}}{\mathrm{d}R}$ and $A_2 = R_0 \frac{\mathrm{dNu}_T}{\mathrm{d}R}$, where the derivatives are evaluated at $R = R_0$.

When the average in Equations 13 and 14 is interpreted as a horizontal average, the model of Traxler et al. (2011b) recovers the γ-instability theory of Radko (2003). Indeed, in that case, $\bar{w} = 0$ by mass conservation, and the momentum equation reduces to $\partial \bar{\mathbf{u}}/\partial t = \mathrm{Pr}\nabla^2 \bar{\mathbf{u}}$ so that any horizontal mean flow must decay viscously. The remaining mean-field equations are

$$\frac{\partial \bar{T}}{\partial t} = -\frac{\partial F_T^{\mathrm{tot}}}{\partial z} \text{ and } \frac{\partial \bar{C}}{\partial t} = -\frac{\partial F_C^{\mathrm{tot}}}{\partial z}, \qquad 16.$$

where $F_T^{\mathrm{tot}} = F_T - 1$ and $F_C^{\mathrm{tot}} = F_C - \tau R_0^{-1}$ are the sum of the turbulent and diffusive fluxes of temperature and composition, respectively. Radko (2003) showed that these equations exhibit instability when the total flux ratio $\gamma_{\mathrm{tot}} = F_T^{\mathrm{tot}}/F_C^{\mathrm{tot}}$ is a decreasing function of the density ratio. When this is the case, an interesting phenomenon occurs whereby even though the turbulent fluxes of temperature and composition are individually both down gradient, they combine to act antidiffusively. As such, the γ-instability suffers from an ultraviolet catastrophe, which is regularized on scales that approach the basic instability scale (where the assumed flux laws no longer apply; see Traxler et al. 2011b). The horizontally invariant γ-instability modes are precursors to layering and therefore are often called layering modes.

When the average in Equations 13 and 14 is instead interpreted as an ensemble average, and the 3D structure of the normal modes is retained, the model of Traxler et al. (2011b) also captures the dynamics of the collective instability (Stern 1969, Holyer 1981) as a distinctively different positive feedback loop. As clarified by Radko (2013), the collective instability can be viewed as a turbulent version of the ODDC instability and excites large-scale internal gravity waves. Indeed, the turbulent compositional flux in fingering convection is always larger than the turbulent heat flux (e.g., $\gamma < 1$). If $\mathrm{Nu}_T \gg 1$ and $\mathrm{Nu}_C \gg 1$, then the turbulent flux is a significant component of the total flux. As a result, the unstably stratified component becomes the fastest diffusing one, a situation that exactly reproduces ODDC, albeit from a turbulent perspective.

The predictions of Traxler et al. (2011b) agree very well with high-Pr numerical experiments (Stellmach et al. 2011), both for the γ-instability and for the collective instability, as long as the typical wavelength of the mean-field mode exceeds five or more wavelengths of the basic fingering instability. These experiments therefore provide further empirical justification for the assumptions made in constructing the closure model above.

3.2.2. Application to low–Prandtl number fingering convection. The theory of Traxler et al. (2011b) applies in all generality to both high- and low-Pr fingering convection and ODDC. In the low-Pr limit, the semi-analytical flux laws proposed by Brown et al. (2013) can be used to estimate F_T and F_C (using Equations 11 and 12) and then to systematically analyze the stability of spatially homogeneous fingering convection to large-scale mean-field instabilities across parameter space. Results were presented by Garaud et al. (2015) in the context of applications of fingering convection to stellar astrophysics but are of course more generally applicable to liquid metals as well. They are illustrated in **Figure 4**. One of the most important findings of this investigation is that the γ-instability, responsible for the excitation of layering modes, is never active in low-Pr fingering convection (see also Traxler et al. 2011a). This is because turbulent fluxes always remain relatively small, so the total flux ratio γ_{tot} (which controls the development of the γ-instability; see above) is

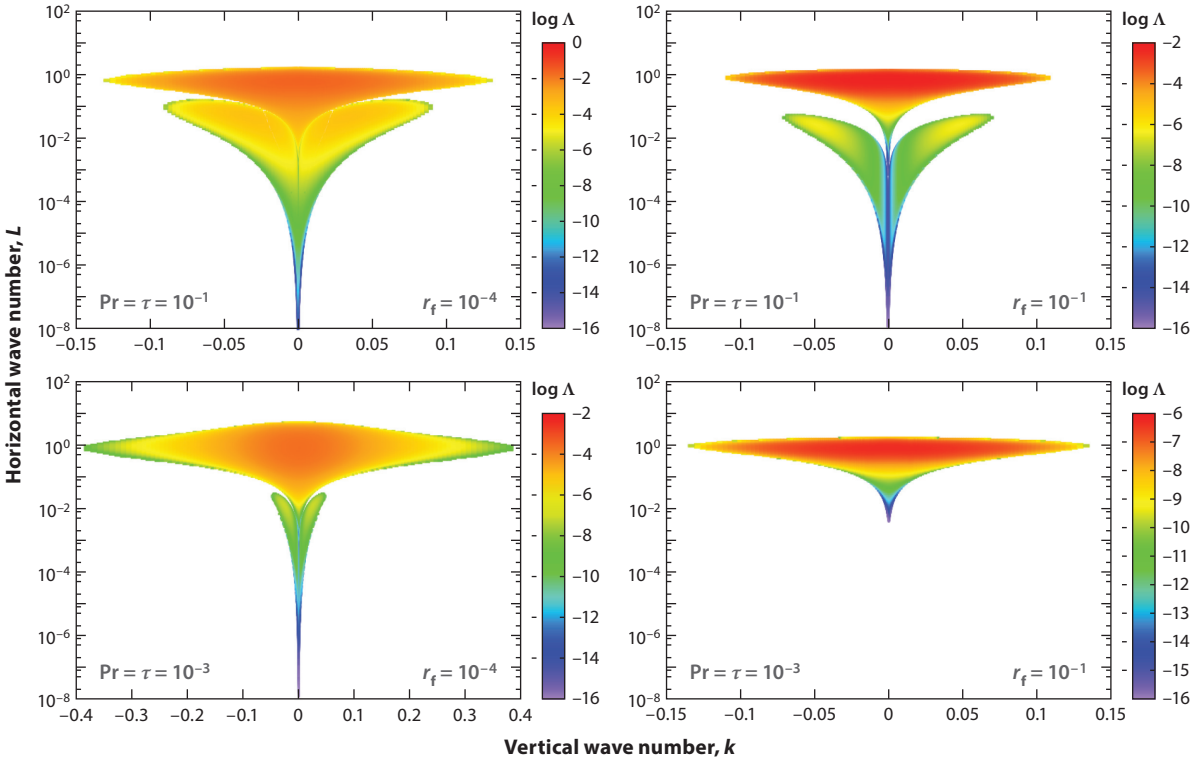

Figure 4

Results of the mean-field theory analysis for four sets of input parameters. In each panel, the color represents the logarithm of the growth rate of a growing mode (*white* represents decaying modes). The vertical wave number k is plotted on a linear x-axis, and the total horizontal wave number L is plotted on a logarithmic y-axis, giving the results their appealing flower-like shape (Traxler et al. 2011b). The bulbs are modes with $L \sim \mathcal{O}(1)$, which are basic fingering modes. When unstable, the γ-modes would appear as modes with $L \ll 1$ for a wide range of k, but are clearly absent here. The leaves, when present, are the collective instability modes. The collective instability disappears for Pr, $\tau < 10^{-3}$, and for a larger reduced density ratio $r_\mathrm{f} = (R_0 - 1)(\tau^{-1} - 1)^{-1}$.

close to the diffusive flux ratio $\gamma_\mathrm{diff} = R_0\tau^{-1}$. Because γ_diff increases linearly with the density ratio, this situation is stable to the γ-instability.

In contrast, the collective instability can be active, but only for a sufficiently low density ratio and relatively large Prandtl number (Pr $\sim 10^{-3}$ or more, which precludes stellar applications, but could be relevant for liquid metals); again, this is because the instability requires relatively large turbulent fluxes to take place. The typical scale of the collective modes varies widely with input parameters, but the fastest-growing ones are typically $\mathcal{O}(10d)$ or $\mathcal{O}(100d)$ and have $l \sim m \sim k$. When the collective instability does take place, it excites gravity waves that can grow to relatively large amplitude and cause local inversions in the density profile as they break (see **Figure 5**). These inversions appear to cause layering in a manner consistent with the original prediction of Stern (1969) (see also Stern & Simeonov 2002) in the context of oceanic fingering. The layers are formed with a vertical wave number similar to that of the waves that created it, and are horizontally coherent over long distances. The local density gradient is strongly negative (i.e., stably stratified) in the interfaces that separate these layers but nearly neutral within the layers, which are mixed by layer-scale overturning convective eddies. The overall rate of turbulent transport increases somewhat

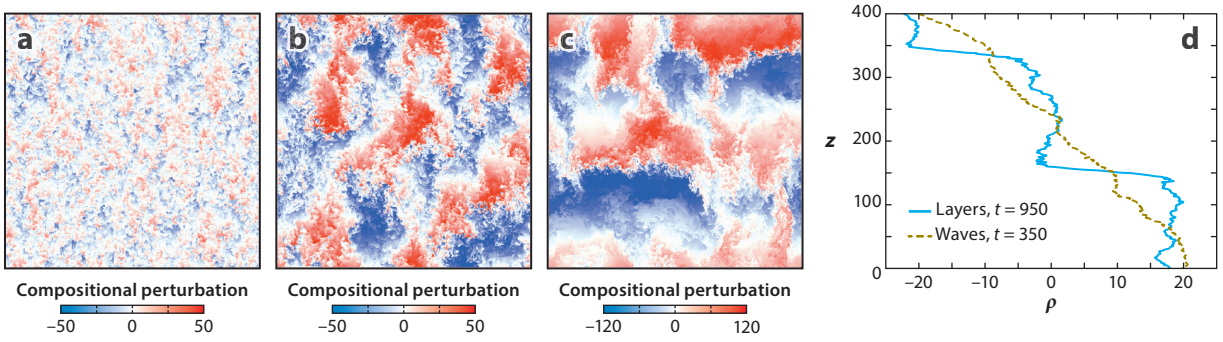

Figure 5

Snapshots of the compositional perturbations in a three-dimensional direct numerical simulation with $\mathrm{Pr} = 0.1$, $\tau = 0.03$, and $R_0 = 1.1$, taken (*a*) after saturation of the basic instability but before the onset of the collective instability, (*b*) once the collective instability has grown to a significant amplitude, and (*c*) after strong breaking events have led to the formation of layers. The horizontally averaged density profiles of panels *b* and *c* are shown in panel *d*. Adapted from Garaud et al. (2015).

when the gravity waves form but increases much more significantly once layered convection sets in. Whether layers have a tendency to merge once they have formed remains to be determined.

4. NONLINEAR SATURATION OF OSCILLATORY DOUBLE-DIFFUSIVE CONVECTION

As discussed in Section 2, low-Pr ODDC typically develops naturally from the basic linear instability, in stark contrast with the high-Pr regime. In this section, for simplicity, I focus on presenting the results of studies of nonlinear ODDC within the linearly unstable range, $1 < R_0^{-1} < \frac{\mathrm{Pr}+1}{\mathrm{Pr}+\tau}$ (see Section 6 for additional effects).

4.1. Saturation of the Basic Instability

The dynamics of ODDC-unstable systems after saturation bear very little resemblance with the properties of the fastest-growing ODDC modes (Mirouh et al. 2012). Saturation appears to proceed through nonlinear wave–wave interactions that promote the emergence of new oscillatory modes that are no longer vertically invariant but are instead much more inclined; their vertical scale becomes $\mathcal{O}(10d)$, and their horizontal scale is now much larger (usually domain scale in most simulations). Their oscillation frequency is correspondingly reduced. The precise nature of this wave–wave interaction remains to be determined (Moll et al. 2016).

Under the adopted triply periodic model setup, both turbulent fluxes of temperature and composition must be positive when nonlinear ODDC is statistically stationary, because in that limit $\langle wT \rangle = \langle |\nabla T|^2 \rangle$ and $R_0^{-1} \langle wC \rangle = \tau \langle |\nabla C|^2 \rangle$. They are now related to the respective Nusselt numbers via

$$\mathrm{Nu}_T = 1 + \langle wT \rangle \text{ and } \mathrm{Nu}_C = 1 + \frac{R_0}{\tau} \langle wC \rangle. \qquad 17.$$

Mirouh et al. (2012) reported experimental measurements of the turbulent temperature flux in nonlinear ODDC just after saturation of the basic instability. An empirical fit to the data shows that they can be modeled by the formula

$$\langle wT \rangle = \mathrm{Nu}_T - 1 = (0.75 \pm 0.05)\mathrm{Sc}^{0.25 \pm 0.15} \frac{1-\tau}{R_0^{-1}-1}(1-r_o), \qquad 18.$$

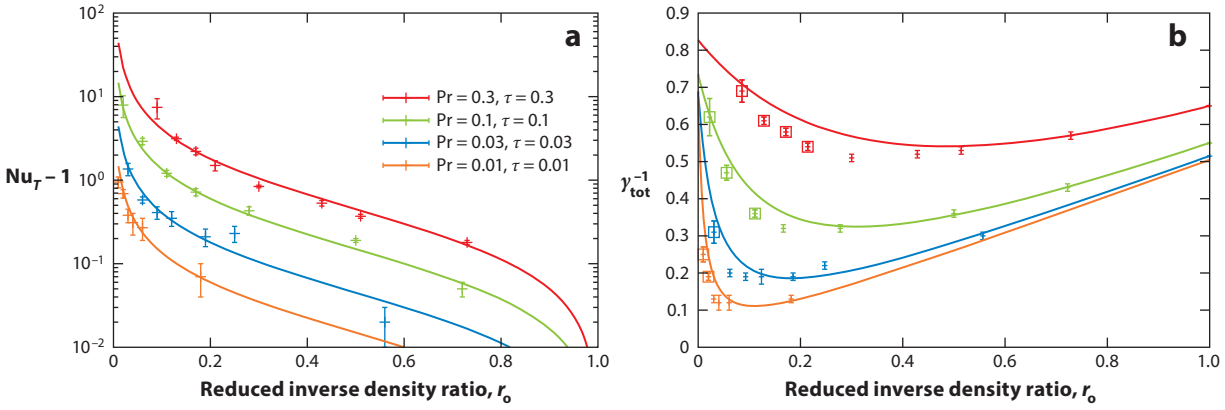

Figure 6

(*a*) Temperature Nusselt number as a function of the reduced inverse density ratio r_o, for Pr = τ values of 0.3 (*red*), 0.1 (*green*), 0.03 (*blue*), and 0.01 (*orange*). The data points are from Mirouh et al. (2012), and the lines correspond to the model of Equation 18. (*b*) Variation of the total inverse flux ratio $\gamma_{\rm tot}^{-1}$ with r_o. The data points are from Mirouh et al. (2012) and the lines can be deduced from the model of Equations 18 and 19. The large symbols mark simulations that eventually show spontaneous layering. Note how they all lie on the decreasing part of the $\gamma_{\rm tot}^{-1}$ curves.

for Pr and τ ranging from 0.01 to 0.3, and for a reduced inverse density ratio $r_o = (R_0^{-1} - 1)(\frac{\rm Pr+1}{\rm Pr+\tau} - 1)^{-1}$ ranging from 0.01 to about 0.8. The formula must clearly break down as $R_0^{-1} \to 1$ and should be discarded in that limit. The turbulent flux ratio γ can be estimated using an extension of the theory of Schmitt (1979) applied to ODDC and yields (Mirouh et al. 2012)

$$\gamma = \frac{\langle wT \rangle}{\langle wC \rangle} = R_0 \frac{\lambda_{R,\max} + L_{\max}^2}{\lambda_{R,\max} + \tau L_{\max}^2} \cdot \frac{(\lambda_{R,\max} + \tau L_{\max}^2)^2 + \omega_{\max}^2}{(\lambda_{R,\max} + L_{\max}^2)^2 + \omega_{\max}^2}, \qquad 19.$$

where $\lambda_{R,\max}$ and $\omega_{\max}$ are the real and imaginary parts of the growth rate of the fastest growing mode, respectively, and $L_{\max}$ is their corresponding horizontal wave number. The compositional Nusselt number and the inverse total flux ratio can then be easily calculated from Nu_T and γ using $\mathrm{Nu}_C = 1 + R_0 \langle wT \rangle / \gamma\tau$ and $\gamma_{\rm tot}^{-1} = \tau R_0^{-1} \mathrm{Nu}_C / \mathrm{Nu}_T$. **Figure 6** shows both models in comparison with the data; the fit is adequate, although not perfect, across the parameter space explored. Whether it still holds for much lower values of Pr and τ remains to be determined.

4.2. Beyond the Saturation of the Basic Instability

Until recently, very little was known about the behavior of low-Pr ODDC beyond the saturation of the basic instability. Models proposed in the astrophysical literature assumed that it would either always remain in a state dominated by small-scale turbulence (Stevenson 1977, Langer et al. 1983) or take the form of layered convection (by analogy with observations of nonlinear ODDC in geophysics) with either a single interface (Stevenson 1982) or a density staircase (Stevenson 1985, Spruit 1992, Chabrier & Baraffe 2007, Leconte & Chabrier 2012, Spruit 2013).

However, as discovered by Rosenblum et al. (2011) using DNSs, ODDC can exhibit all of these phenomena beyond the saturation of the basic instability, depending on the regime considered. Ubiquitous spontaneous layering is observed in the less stably stratified cases (R_0^{-1} closer to one), whereas the more stably stratified ones (R_0^{-1} closer to marginal stability) continue to undergo some form of weak wave turbulence, with further transfer of energy to larger scales after saturation. This dichotomy between low- and high-R_0^{-1} systems is illustrated in **Figure 7**. Rosenblum

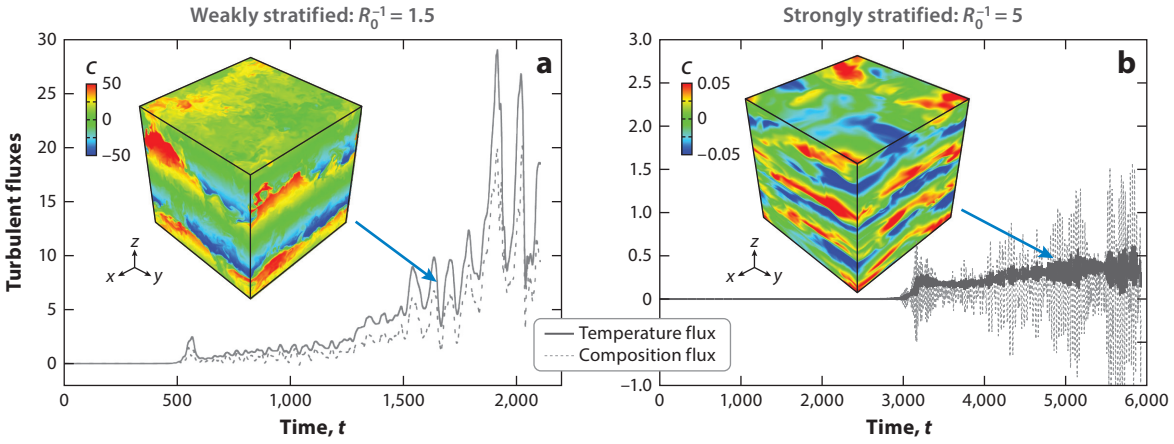

Figure 7

Illustrative simulations of oscillatory double-diffusive convection for $\mathrm{Pr} = \tau = 0.03$ in (*a*) the weakly stratified case ($R_0^{-1} = 1.5$) and (*b*) the strongly stratified case ($R_0^{-1} = 5$). In each panel, the lines represent the turbulent fluxes of temperature (*solid lines*) and composition (*dotted lines*), whereas the images are representative snapshots of the compositional perturbations. In both panels, the fluxes grow exponentially, saturate briefly, and then continue to grow on a longer timescale. In panel *a*, the growth is significant and stepwise, each successive step corresponding to the formation and then merging of convective layers until only one remains. In panel *b*, the growth is much milder and is associated with the gradual coarsening of the dominant gravity waves. The low-R_0^{-1} snapshot is in a temporary two-layer state, with two turbulent interfaces and high-amplitude perturbations. By contrast, the high-R_0^{-1} snapshot is in a statistically stationary state, with small-amplitude but large-scale gravity waves that are strongly inclined towards the horizontal. Adapted from Mirouh et al. (2012).

et al. (2011) concluded that a quantitative model of ODDC must contain (*a*) a criterion to determine which outcome to expect, (*b*) a model for layered ODDC, and (*c*) a model for nonlayered ODDC.

4.2.1. Spontaneous layer formation in oscillatory double-diffusive convection. Rosenblum et al. (2011) showed that layering in ODDC arises from the same γ-instability mechanism known to cause layering in high-Pr fingering convection (see Section 3.2.1) (Radko 2003). The mean-field equations applied to horizontally invariant perturbations are the same for ODDC and fingering convection (because the term $\pm\bar{w}$ in Equation 14 is zero by mass conservation), so the γ-instability proceeds in exactly the same way, provided that the total flux ratio γ_{tot} is a decreasing function of the density ratio R_0 (or, equivalently, that $\gamma_{\mathrm{tot}}^{-1}$ is a decreasing function of R_0^{-1}). As shown in **Figure 6**, all the simulations where $\frac{d\gamma_{\mathrm{tot}}^{-1}}{dR^{-1}} < 0$ do indeed transition to layered convection (see Section 4.2.2).

Using their empirically derived flux models (i.e., Equations 18 and 19) to inform the mean-field equations, Mirouh et al. (2012) were able to predict the growth rate of layering modes with any given vertical wave number k, for a range of parameters Pr, τ, and R_0^{-1}. The predictions fit the observed growth rates of layering modes in selected simulations remarkably well for sufficiently small wave numbers (e.g., see **Figure 8*a***). More generally, Mirouh et al. (2012) also identified the region of parameter space prone to spontaneous layering. The results are shown in **Figure 8*b*** and reveal that the critical inverse density ratio below which the γ-instability takes place increases significantly as τ and Pr decrease, suggesting that the latter may be quite common at low Pr and low τ.

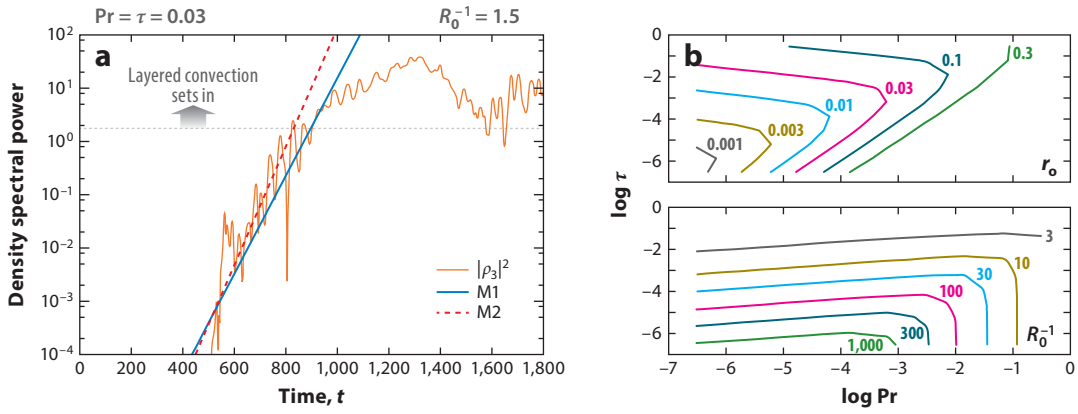

Figure 8

(*a*) Amplitude as a function of time of the initial three-layer mode observed in the simulation with Pr = τ = 0.03 and R_0^{-1} = 1.5 shown in **Figure 7** (*solid orange line*), compared with the prediction from the γ-instability theory using experimentally determined measurements of F_T and γ (*solid blue line*), the prediction from the γ-instability theory using the flux laws for F_T and γ given in Equations 18 and 19 (*dashed red line*), and the amplitude above which layered convection sets in (*horizontal dashed gray line*). (*b*) Contour plots of the critical reduced inverse density ratio for layering (*top*) and the critical inverse density ratio for layering (*bottom*) as a function of Pr and τ. Adapted from Mirouh et al. (2012).

4.2.2. Layered convection at low R_0^{-1}. Layering following the development of the γ-instability proceeds as follows. The exponential growth of the layering modes gradually weakens the background density stratification. Eventually, inversions in the density profile locally appear, at which point layered convection sets in (Rosenblum et al. 2011, Mirouh et al. 2012). The layer height is initially equal to the wavelength of the dominant layering mode, which turns out to be between 30*d* and 50*d* across most of the parameter space studied. As in the layered fingering case described in Section 3.2.2, the horizontally averaged density profile is close to neutrally stratified in the convective layers and is stably stratified within the interfaces, thus taking the form of a staircase. Convective eddies span each layer and mix them efficiently in a manner somewhat reminiscent of Rayleigh–Bénard convection between stress-free parallel plates. The analogy rapidly breaks down, however, as the interfaces between each layer are not rigid but can instead be viewed as thin and very mobile material surfaces that support the propagation of high-amplitude interfacial gravity waves and are occasionally pierced by strong updrafts or downdrafts. This is in striking contrast with observations of layered ODDC in the geophysical context, where the interfaces are quiescent and flat, and invalidates prior models for layered convection at low Pr that assumed that interfacial transport is diffusive (Spruit 1992, Leconte & Chabrier 2012).

In addition, spontaneously emerging staircases in low-Pr ODDC are not in equilibrium. In the DNSs shown in **Figure 7** (see also **Supplemental Video 1**), as in all cases seen to date (Wood et al. 2013), the layers always proceed to merge until only one is left in the domain (at which point the mergers necessarily cease). The merger timescale seems to depend on their separation as well as on the global system parameters, but the cause of the mergers remains to be determined. Whether this ubiquitous coarsening process is an inherent property of layered convection in ODDC, or whether it is partially related to the model assumptions (i.e., Boussinesq approximation and periodic perturbations) or the parameters selected, also remains to be determined.

Supplemental Material

Turbulent fluxes in the layered phase can be orders of magnitude larger than in the nonlayered phase and increase with each layer merger (see **Figures 7** and **9*a***). Wood et al. (2013) quantified the transport of temperature and composition in layered ODDC using DNSs. They found that the

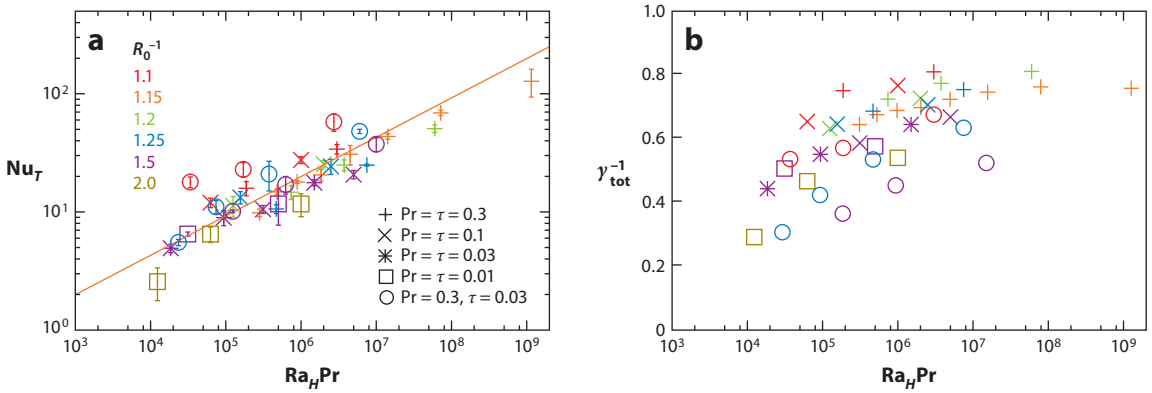

Figure 9

Variation of (*a*) Nu_T and (*b*) $\gamma_{\mathrm{tot}}^{-1}$ with $\mathrm{Ra}_H\,\mathrm{Pr}$, R_0^{-1}, Pr, and τ in all simulations exhibiting spontaneous layering available to date. Data taken from Wood et al. (2013).

thermal Nusselt number scales with the Rayleigh number based on the dimensional layer height H as

$$\mathrm{Nu}_T - 1 = f(R_0^{-1}, \tau)(\mathrm{Ra}_H\,\mathrm{Pr})^{1/3}, \qquad 20.$$

where

$$\mathrm{Ra}_H = \left(\frac{H}{d}\right)^4 = \frac{\alpha g \left|\frac{\mathrm{d}T_0}{\mathrm{d}z} - \frac{\mathrm{d}T_{\mathrm{ad}}}{\mathrm{d}z}\right| H^4}{\kappa_T \nu},$$

and where $f(R_0^{-1}, \tau)$ is a function that depends weakly on R_0^{-1} and τ (to be precise, its dependence is too weak to identify unambiguously from the available data) but takes values around 0.1 for Pr and τ between 0.01 and 0.3 and for R_0^{-1} between 1 and 2. The scaling $\mathrm{Nu}_T - 1 \propto (\mathrm{Ra}_H\,\mathrm{Pr})^{1/3}$ is not entirely surprising. The dependence of $\mathrm{Nu}_T - 1$ on $\mathrm{Ra}_H^{1/3}$ recovers the scaling derived on dimensional grounds by Turner (1965) for the transport of heat across a single sharp diffusive interface. The dependence on $\mathrm{Ra}_H\,\mathrm{Pr}$ accounts for the fact that viscosity is not expected to play any role on the scales associated with the thermal interface at low Pr and confirms one of the central predictions of Spruit's (1992, 2013) models.

Wood et al. (2013) also found that $\gamma_{\mathrm{tot}}^{-1}$ in layered ODDC has a complex dependence on all input parameters, as well as on the layer height. In each simulation, $\gamma_{\mathrm{tot}}^{-1}$ increases gradually with each merger and asymptotes to a constant that seems to depend more sensitively on R_0^{-1} and Sc than on τ. This constant likely represents the value of the total inverse flux ratio across a single interface in an infinite domain, which had been estimated to be equal to $\gamma_{\mathrm{tot}}^{-1} = \tau^{1/2}$ in high-Pr layered double-diffusive convection by Linden & Shirtcliffe (1978). However, Wood et al. (2013) and Moll et al. (2018) found that this high-Pr model does not apply in low-Pr staircases (where it would largely underestimate $\gamma_{\mathrm{tot}}^{-1}$), which is not surprising given the turbulent nature of the low-Pr interfaces compared with the laminar high-Pr ones. This calls for a revision of many of the previously proposed models for layered convection at low Pr (e.g., Stevenson & Salpeter 1977, Spruit 1992, Leconte & Chabrier 2012), which all rely on $\gamma_{\mathrm{tot}}^{-1} = \tau^{1/2}$ to estimate the compositional flux through an interface.

4.2.3. Oscillatory double-diffusive convection at high R_0^{-1}. In the more stably stratified case, layers cannot form spontaneously from the γ-instability because $\gamma_{\mathrm{tot}}^{-1}$ increases with R_0^{-1}. Instead,

nonlinear ODDC remains in a state of weak wave-dominated turbulence and, as shown by Moll et al. (2016), the turbulent fluxes are always fairly weak (both temperature and compositional Nusselt numbers remain of order unity). Interesting dynamics nevertheless take place, in which the nonlinear interactions between the waves appear to drive an inverse energy cascade to larger scales. Once a statistically stationary state has been reached, most of the energy becomes concentrated in a few dominant gravity-wave modes. These typically span the entire computational domain horizontally and have a vertical wavelength between $30d$ and $50d$, regardless of the domain size or aspect ratio.

In some cases, significant energy is channeled into horizontally invariant shearing modes that interact with the waves in a manner reminiscent of relaxation oscillations (Paparella et al. 2002, Moll et al. 2016). The term shearing mode here is loosely used to describe any horizontally invariant mode. These are not naturally excited by the linear ODDC instability, so their growth must necessarily arise from the nonlinear interaction between gravity waves. Once a shearing mode reaches a significant amplitude, however, it becomes detrimental to the ODDC instability and suppresses the waves that generated it. The shear then decays viscously, and the wave field gradually recovers, at which point the cycle repeats. When present, this interaction is associated with significant intermittency in the overall transport rates of both temperature and composition. This phenomenon is not ubiquitous, however. In many cases, the shearing modes never acquire significant energy, and the dynamics remain dominated by large-scale gravity waves at all times.

5. ASTROPHYSICAL APPLICATIONS OF LOW-Pr DOUBLE-DIFFUSIVE CONVECTION

Having outlined what is currently known from theory about double-diffusive convection at low Pr, I now turn to its applications to astrophysics (see, for instance, Copley et al. 1970 for metallurgical applications). The importance of double-diffusive convection in this context was first reviewed by Spiegel (1969). He summarized various possible impacts of both fingering convection and ODDC across stellar astrophysics and established the close relationship between ODDC and the phenomenon already known in this context as semiconvection (see also Schwarzschild & Härm 1958, Kato 1966). Until recently, however, the study of double-diffusive mixing in stars and planets remained on the fringe, perhaps because standard stellar and planetary models (which ignore it) were so successful in explaining most available observations.

This has changed dramatically in the past 10 years. Planetary science has been revolutionized by the development and implementation of new technologies for detection and remote sensing of exoplanets, as well as the various NASA missions to our own Solar System's giant planets. Stellar astrophysics has similarly undergone a recent transformation with the development of asteroseismology (which directly probes the internal structure of stars) together with high-precision spectroscopy. In all cases, new data have come to light that present significant challenges to standard theories of planetary and stellar structure and evolution, often revealing the need for improved thermocompositional mixing models. Astrophysicists have therefore turned to double-diffusive convection to see if it may explain some of the discrepancies between models and observations. This question is pertinent since double-diffusive mixing should be ubiquitous in stars and planets. As reviewed in Section 2, the range of density ratios unstable to fingering convection is $1 < R_0 < \tau^{-1}$, while the range of inverse density ratios unstable to ODDC is $1 < R_0^{-1} < \frac{\mathrm{Pr}+1}{\mathrm{Pr}+\tau}$. In regions of the interiors of giant planets where hydrogen is in metallic form, one finds that $\mathrm{Pr} \sim \tau \sim 10^{-2}$, while in the stably stratified regions of stellar interiors, we have $\mathrm{Pr} \sim \tau \ll 10^{-5}$. This implies that a very slightly unstable compositional gradient can destabilize a stable thermal stratification, and a very slightly unstable thermal gradient can destabilize a stable compositional gradient.

Compositional gradients in astrophysics can be helium concentration gradients in a hydrogen-rich plasma or gradients of various species of higher atomic weight (often referred to as metallicity in stellar astrophysics) within a hydrogen–helium mixture. Stable compositional gradients are ubiquitous in stars because the majority of nuclear reactions are fusion reactions that increase the mean atomic weight of the material and usually take place in the core. By contrast, unstable compositional gradients are less common but can arise through a few unusual nuclear reactions that decrease the mean atomic weight, in off-center burning, or through the accretion of material at the surface of the star. In the remainder of this section I discuss some of the impacts of the findings reported in Sections 3 and 4 on a few selected problems in astrophysics.

5.1. Fingering Convection (Thermohaline Convection) in Stars

Fingering convection is commonly referred to as thermohaline convection in astrophysics (even though the slowly diffusing component is not salt). One of the earliest applications of fingering convection discussed in stars takes place during their evolution on the red giant branch (RGB). Ulrich (1972) noted that the nuclear reaction $^3\mathrm{He} + {}^3\mathrm{He} \rightarrow {}^4\mathrm{He} + \mathrm{p} + \mathrm{p}$ is one of the rare reactions that decreases the mean atomic weight per particle. It is known to take place on the outskirts of the hydrogen-burning shell in RGB stars and gradually causes the development of an unstable compositional gradient above the shell. Fingering convection then develops and can mix material from the shell upward. If it is sufficiently strong, the mixed layer ultimately spans the entire stable region between the burning shell and the outer convection zone, bringing products and by-products of nuclear reactions to the surface. Charbonnel & Zahn (2007) first put forward this effect to explain some of the peculiar abundance changes observed by Gratton et al. (2000) in stars climbing up the RGB. They used the abundance data to calibrate traditional models for mixing by fingering convection (see Section 3.1.2) and found that the model of Ulrich (1972) could indeed explain the observations. In an interesting twist, however, that model tends to overestimate mixing measured in DNSs by two orders of magnitude (Brown et al. 2013), which suggests that some yet unaccounted for effect (such as rotation, layering, magnetic fields, or shear) must be present to substantially enhance mixing by fingering convection in RGB stars.

Unstable compositional gradients can also develop from the accretion of high-metallicity material on the surface of a star. This phenomenon was originally proposed in the context of mass transfer in binaries stars (e.g., Stothers & Simon 1969, Stancliffe et al. 2007) but has recently gained a lot of interest in the search for extrasolar planets. During the process of forming an exoplanetary system, it is quite common that one or more planets may fall into a star and pollute its surface with heavy elements. One may therefore wonder whether this could be the explanation for the observed correlation between a star's surface metallicity and its likelihood of having planets (Fischer & Valenti 2005). However, as pointed out by Vauclair (2004), the unstable compositional gradient would drive fingering convection and drain the accreted material deep into the interior of the star. This shortens the surface residence timescale of chemical tracers of planetary impact down to a few hundred thousand years or less (Garaud 2011), showing that the statistically higher metallicity of planet-bearing stars must be of primordial origin.

5.2. Oscillatory Double-Diffusive Convection (Semiconvection) in Planets and Stars

ODDC and its nonlinear manifestations (usually referred to as semiconvection in stellar astrophysics) are thought to occur in compositionally segregated giant planets and in core-convective main sequence stars, as well as in more evolved high-mass stars.

Stevenson was the first to realize and study the importance of ODDC in the evolution of giant planets. He found that there are (at least) two regions where stable compositional gradients and therefore ODDC can be found. The first is located at a pressure of about 1 Mbar, where helium can condense into droplets and rain into the interior. Stevenson & Salpeter (1977) noted that convection is likely partially inhibited by the strong helium gradient that forms in the He rain region, and drew the analogy with ODDC. Limitations on the transport of heat across this region can delay the global cooling of the planet, an effect that may be a possible cause of the unexpectedly high luminosity of Saturn (Stevenson & Salpeter 1977, Fortney & Hubbard 2003). The second region with strong compositional gradients is the interface between the central core (composed of water, silicates, iron, etc.) and the hydrogen/helium envelope. Although this compositional gradient may be strong enough to inhibit regular convection, Stevenson (1982) argued that double-diffusive convection could gradually erode the core over time. He estimated the erosion rate, arguing that a fraction $\gamma_{\rm tot}^{-1}$ of the total convective energy can be used to mix heavy elements upward into the envelope. Using the high-Pr estimates for $\gamma_{\rm tot}^{-1} = \tau^{1/2}$ (Linden & Shirtcliffe 1978), Guillot et al. (2004) showed that the erosion of Jupiter's core would be almost complete after 5 Gyr, whereas that of Saturn would only be partial. These results are consistent with present estimates of the core sizes of both planets but should be revisited given the more recent findings of Wood et al. (2013) and Moll et al. (2018) for low-Pr layered convection. Compositional gradients near the core can also regulate the transport of heat, which in turn affects the thermal evolution of the planet (Stevenson 1985; Chabrier & Baraffe 2007; Leconte & Chabrier 2012, 2013).

In stellar interiors, ODDC usually takes place in compositionally stable regions, located at the outskirts of convective cores, that have formed either because the core has retreated over time or because weak nuclear burning takes place outside the core (e.g., reviewed in Merryfield 1995). Mixing beyond the convective core has important consequences for stars, as it can continually provide them with more fuel, thus prolonging the duration of core-burning phases of stellar evolution. The ultimate size of the core of a star also controls its post–main sequence evolution in sometimes dramatic fashion, especially for high-mass stars (Stothers & Chin 1968, Lauterborn et al. 1971, Langer & Maeder 1995, Straniero et al. 2003, Sukhbold & Woosley 2014). As shown by Moore & Garaud (2016), ODDC in this context always lies in the regime that is unstable to layering. Furthermore, the rate of transport by layered convection is so efficient that it rapidly homogenizes the entire semiconvective layer, which then becomes part of the convective core. Moore & Garaud (2016) thus established that the extent of the convectively mixed core is ultimately more accurately estimated using the Schwarzschild criterion than the Ledoux criterion. Recent asteroseismic data generally confirm this finding (Deheuvels et al. 2016) and further suggest the existence of substantial mixing beyond the edge of the convective zone.

6. NEW PHYSICS AND FUTURE WORK

Previous sections of this review focused on describing the nonlinear dynamics of double-diffusive convection at low Pr as they arise from infinitesimal perturbations. The effects of rotation, shear, lateral gradients, and magnetic fields were all neglected, as was the possibility of finite-amplitude instabilities. However, they are likely very significant in astrophysical applications, and it is worth reviewing, at least very briefly, what is known to date about their impact on low-Pr double-diffusive convection.

The effects of shear on fingering convection and ODDC are nontrivial. Sufficiently strong shear can naturally drive shear instabilities that entirely dominate the double-diffusive dynamics of the system. Weak shear, on the other hand, can interact in complex ways with the developing

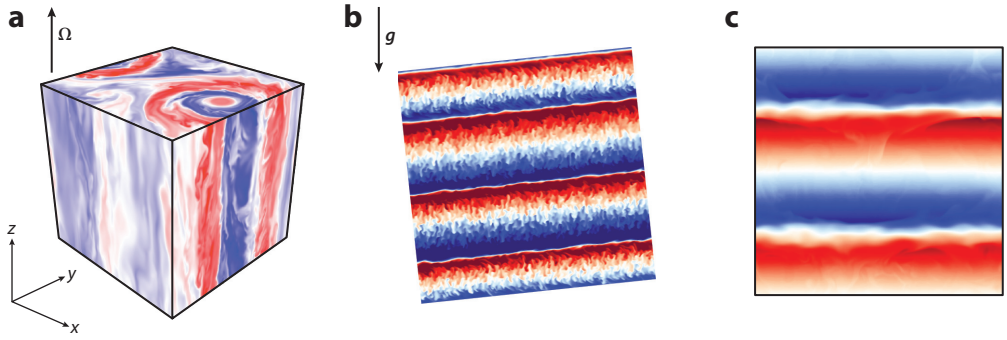

Figure 10

Illustrative snapshots of the compositional perturbations in three different direct numerical simulations. (*a*) Rotating oscillatory double-diffusive convection (ODDC) at $\mathrm{Pr} = \tau = 0.1$, $\mathrm{Ta}^* = 10$, and $R_0^{-1} = 1.25$, showing the presence of a domain-scale vortex that strongly enhances double-diffusive transport. Adapted from Moll & Garaud (2017). (*b*) Intrusions formed as a result of compensating lateral gradients of temperature and composition at $\mathrm{Pr} = \tau = 0.3$ and $R_0 = 5$. Adapted from Medrano et al. (2014). (*c*) Layered ODDC formed by finite-amplitude instability at $\mathrm{Pr} = \tau = 0.03$ and $R_0^{-1} = 7.87$. Simulation from Moll et al. (2018).

double-diffusive instabilities and either promote them or suppress them (e.g., see Linden 1974, Radko 2016, at high Pr). Whether this is the case at low Pr remains to be determined. Similarly, very little is known about the interaction between double-diffusive convection and magnetic fields. It is worth noting that magnetic fields themselves can indirectly affect the buoyancy of a parcel of fluid and therefore play a role analogous (but not identical) to composition in driving double-diffusive instabilities in thermally stratified but chemically homogeneous plasmas (Hughes & Weiss 1995).

Rotation also has nontrivial effects on the dynamics of double-diffusive convection (Pearlstein 1981). These are relatively mild in the linear regime (where rotation merely stabilizes modes that are not invariant in the direction of rotation) but become very substantial beyond the saturation of the basic instability. At low Pr, the influence of rotation can be quantified by the modified Taylor number $\mathrm{Ta}^* = 4\Omega^2 d^4/\kappa_T^2$ (where Ω is the rotation rate) introduced by Moll & Garaud (2017), which happens to be a relatively good estimate of the inverse-square Rossby number of the turbulent flow around the time of saturation of the basic instability. If $\mathrm{Ta}^* \ll 1$, the system dynamics remain relatively unaffected by rotation. If $\mathrm{Ta}^* \gg 1$, rotation significantly influences transport, sometimes reducing it, and sometimes enhancing it compared with nonrotating cases. Most notably, it can suppress the formation of layers in ODDC (and therefore quench transport) but can also cause the emergence of domain-scale vortices within which transport is greatly enhanced (see **Figure 10*a***), in both fingering convection and ODDC (Moll & Garaud 2017; S. Sengupta & P. Garaud, unpublished manuscript). A comprehensive theory of rotating double-diffusive convection at low Pr remains to be developed.

Lateral gradients of temperature and composition can occur even if the background density profile is horizontally invariant, as long as they are density compensating. When this is the case, a new mode of double-diffusive instability emerges that is unstable at all density ratios (in both fingering and ODDC cases). Holyer (1983) presented the theory behind this small-scale intrusive mode and Medrano et al. (2014) explored the theory in the context of low-Pr systems, both linearly and nonlinearly using DNSs (see **Figure 10*b***).

Finally, although I have focused on describing the nonlinear dynamics of low-Pr double-diffusive convection as they arise from infinitesimal perturbations, other outcomes can be achieved if finite-amplitude perturbations are applied to the system, in particular, if these force the latter

into a layered state (Veronis 1965, Huppert & Moore 1976, Proctor 1981, Zaussinger & Spruit 2013). In this case, statistically stationary layered double-diffusive convection can be achieved even in cases that are not prone to any large-scale instabilities, both in fingering convection (any density ratio) and in ODDC (at high inverse density ratio). Moll et al. (2018) present a preliminary study of finite-amplitude layering in low-Pr ODDC (see **Figure 10*c***). Their findings bear many similarities but also some differences with the high-Pr layered ODDC observed in geophysics. At large values of R_0^{-1} (where layers cannot form through the γ-instability), the interfaces are much more quiescent, and transport across the interface is essentially diffusive. The interfaces thicken relative to the layer size as R_0^{-1} increases, but the total inverse flux ratio $\gamma_{\rm tot}^{-1}$ remains relatively independent of R_0^{-1}. Both of these results are similar in the high-Pr regime. Interestingly, however, it appears that $\gamma_{\rm tot}^{-1} \simeq \frac{\rm Pr+1}{\rm Sc+1}$ instead of $\tau^{1/2}$ found at high Pr (Linden & Shirtcliffe 1978). This finding may have significant implications for planetary structure and evolution models, as discussed in Section 5.

SUMMARY POINTS

1. Double-diffusive convection at low Pr is important in stellar and planetary astrophysics and in metallurgy. It differs significantly from the high-Pr regime.
2. Mixing in low-Pr fingering convection can be modeled using simple semi-analytical physically motivated prescriptions, and large-scale instabilities are rare.
3. ODDC in weakly stratified systems spontaneously evolves into layered convection through the γ-instability. The thermocompositional staircases that form in that case are less stable than at high Pr, and transport is very efficient. Mixing in strongly stratified systems is essentially negligible unless layered convection can be mechanically triggered.

FUTURE ISSUES

1. A model for the saturation of ODDC should be constructed.
2. A better quantitative understanding of transport in layered convection in ODDC at both low and high R_0^{-1} is needed.
3. The effects of rotation, shear, lateral gradients, magnetic fields, and finite-amplitude instabilities should be investigated and likely matter in astrophysical applications.

DISCLOSURE STATEMENT

The author is not aware of any affiliations, memberships, funding, or financial holdings that might be perceived as affecting the objectivity of this review.

ACKNOWLEDGMENTS

P. Garaud gratefully acknowledges funding from the National Science Foundation (NSF) grants 0807672, 0933759, 1211394, and 1412951 over the past 10 years. All of the simulations presented were run using the PADDI code provided by S. Stellmach on the Pleiades and Hyades clusters purchased using NSF MRI grants.

LITERATURE CITED

Baines P, Gill A. 1969. On thermohaline convection with linear gradients. *J. Fluid Mech.* 37:289–306

Brown JM, Garaud P, Stellmach S. 2013. Chemical transport and spontaneous layer formation in fingering convection in astrophysics. *Astrophys. J.* 768:34

Chabrier G, Baraffe I. 2007. Heat transport in giant (exo)planets: a new perspective. *Astrophys. J. Lett.* 661:L81–84

Charbonnel C, Zahn JP. 2007. Thermohaline mixing: a physical mechanism governing the photospheric composition of low-mass giants. *Astron. Astrophys.* 467:L15–18

Copley SM, Giamei AF, Johnson SM, Hornbecker MF. 1970. The origin of freckles in unidirectionally solidified castings. *Metall. Trans.* 1(8):2193–204

Deheuvels S, Brandão I, Silva Aguirre V, Ballot J, Michel E, et al. 2016. Measuring the extent of convective cores in low-mass stars using Kepler data: toward a calibration of core overshooting. *Astron. Astrophys.* 589:A93

Denissenkov PA. 2010. Numerical simulations of thermohaline convection: implications for extra-mixing in low-mass RGB stars. *Astrophys. J.* 723:563–79

Fischer DA, Valenti J. 2005. The planet-metallicity correlation. *Astrophys. J.* 622:1102–17

Fortney JJ, Hubbard WB. 2003. Phase separation in giant planets: inhomogeneous evolution of Saturn. *Icarus* 164:228–43

Garaud P. 2011. What happened to the other Mohicans? The case for a primordial origin to the planet–metallicity connection. *Astrophys. J. Lett.* 728:L30

Garaud P, Brummell N. 2015. 2D or not 2D: the effect of dimensionality on the dynamics of fingering convection at low Prandtl number. *Astrophys. J.* 815:42

Garaud P, Medrano M, Brown JM, Mankovich C, Moore K. 2015. Excitation of gravity waves by fingering convection, and the formation of compositional staircases in stellar interiors. *Astrophys. J.* 808:89

Gratton RG, Sneden C, Carretta E, Bragaglia A. 2000. Mixing along the red giant branch in metal-poor field stars. *Astron. Astrophys.* 354:169–87

Guillot T, Stevenson DJ, Hubbard WB, Saumon D. 2004. The interior of Jupiter. In *Jupiter: The Planet, Satellites, and Magnetosphere*, ed. F Bagenal, T Dowling, W McKinnon, pp. 35–57. Cambridge, UK: Cambridge Univ. Press

Holyer JY. 1981. On the collective instability of salt fingers. *J. Fluid Mech.* 110:195–207

Holyer JY. 1983. Double-diffusive interleaving due to horizontal gradients. *J. Fluid Mech.* 137:347–62

Hughes DW, Weiss NO. 1995. Double-diffusive convection with two stabilizing gradients: strange consequences of magnetic buoyancy. *J. Fluid Mech.* 301:383–406

Huppert HE, Moore DR. 1976. Nonlinear double-diffusive convection. *J. Fluid Mech.* 78:821–54

Kato S. 1966. Overstable convection in a medium stratified in mean molecular weight. *Publ. Astron. Soc. Jpn.* 18:374–83

Kippenhahn R, Ruschenplatt G, Thomas H. 1980. The time scale of thermohaline mixing in stars. *Astron. Astrophys.* 91:175–80

Krishnamurti R. 2003. Double-diffusive transport in laboratory thermohaline staircases. *J. Fluid Mech.* 483:287–314

Langer N, Fricke KJ, Sugimoto D. 1983. Semiconvective diffusion and energy transport. *Astron. Astrophys.* 126:207–8

Langer N, Maeder A. 1995. The problem of the blue-to-red supergiant ratio in galaxies. *Astron. Astrophys.* 295:685–92

Lauterborn D, Refsdal S, Weigert A. 1971. Stars with central helium burning and the occurrence of loops in the H-R diagram. *Astron. Astrophys.* 10:97–117

Leconte J, Chabrier G. 2012. A new vision of giant planet interiors: impact of double diffusive convection. *Astron. Astrophys.* 540:A20

Leconte J, Chabrier G. 2013. Layered convection as the origin of Saturn's luminosity anomaly. *Nat. Geosci.* 6:347–50

Linden PF. 1974. Salt fingers in a steady shear flow. *Geophys. Astrophys. Fluid Dyn.* 6:1–27

Linden PF, Shirtcliffe TGL. 1978. The diffusive interface in double-diffusive convection. *J. Fluid Mech.* 87:417–32
Medrano M, Garaud P, Stellmach S. 2014. Double-diffusive mixing in stellar interiors in the presence of horizontal gradients. *Astrophys. J. Lett.* 792:L30
Merryfield WJ. 1995. Hydrodynamics of semiconvection. *Astrophys. J.* 444:318–37
Mirouh GM, Garaud P, Stellmach S, Traxler AL, Wood TS. 2012. A new model for mixing by double-diffusive convection (semi-convection). I. The conditions for layer formation. *Astrophys. J.* 750:61
Moll R, Garaud P. 2017. The effect of rotation on oscillatory double-diffusive convection (semiconvection). *Astrophys. J.* 834:44
Moll R, Garaud P, Mankovitch C, Fortney JJ. 2018. Double-diffusive erosion of the core of Jupiter. *Astrophys. J.* In press
Moll R, Garaud P, Stellmach S. 2016. A new model for mixing by double-diffusive convection (semi-convection). III. Thermal and compositional transport through non-layered ODDC. *Astrophys. J.* 823:33
Moore K, Garaud P. 2016. Main sequence evolution with layered semiconvection. *Astrophys. J.* 817:54
Nield DA. 1968. Onset of thermohaline convection in a porous medium. *Water Resour. Res.* 4:553–60
Paparella F, Spiegel EA, Talon S. 2002. Shear and mixing in oscillatory doubly diffusive convection. *Geophys. Astrophys. Fluid Dyn.* 96:271–89
Pearlstein AJ. 1981. Effect of rotation on the stability of a doubly diffusive fluid layer. *J. Fluid Mech.* 103:389–412
Proctor MRE. 1981. Steady subcritical thermohaline convection. *J. Fluid Mech.* 105:507–21
Radko T. 2003. A mechanism for layer formation in a double-diffusive fluid. *J. Fluid Mech.* 497:365–80
Radko T. 2013. *Double-Diffusive Convection*. Cambridge, UK: Cambridge Univ. Press
Radko T. 2016. Thermohaline layering in dynamically and diffusively stable shear flows. *J. Fluid Mech.* 805:147–70
Radko T, Smith DP. 2012. Equilibrium transport in double-diffusive convection. *J. Fluid Mech.* 692:5–27
Rosenblum E, Garaud P, Traxler A, Stellmach S. 2011. Turbulent mixing and layer formation in double-diffusive convection: three-dimensional numerical simulations and theory. *Astrophys. J.* 731:66
Schmitt RW. 1979. The growth rate of super-critical salt fingers. *Deep Sea Res. A* 26:23–40
Schmitt RW. 1983. The characteristics of salt fingers in a variety of fluid systems, including stellar interiors, liquid metals, oceans, and magmas. *Phys. Fluids* 26:2373–77
Schmitt RW, Ledwell J, Montgomery E, Polzin K, Toole J. 2005. Enhanced diapycnal mixing by salt fingers in the thermocline of the tropical atlantic. *Science* 308:685–88
Schwarzschild M, Härm R. 1958. Evolution of very massive stars. *Astrophys. J.* 128:348–60
Shen CY. 1995. Equilibrium salt-fingering convection. *Phys. Fluids* 7:706–17
Spiegel EA. 1969. Semiconvection. *Comments Astrophys. Space Phys.* 1:57
Spiegel EA, Veronis G. 1960. On the Boussinesq approximation for a compressible fluid. *Astrophys. J.* 131:442
Spruit HC. 1992. The rate of mixing in semiconvective zones. *Astron. Astrophys.* 253:131–38
Spruit HC. 2013. Semiconvection: theory. *Astron. Astrophys.* 552:A76
Stancliffe RJ, Glebbeek E, Izzard RG, Pols OR. 2007. Carbon-enhanced metal-poor stars and thermohaline mixing. *Astron. Astrophys.* 464:L57–60
Stellmach S, Traxler A, Garaud P, Brummell N, Radko T. 2011. Dynamics of fingering convection. Part 2. The formation of thermohaline staircases. *J. Fluid Mech.* 677:554–71
Stern ME. 1960. The salt fountain and thermohaline convection. *Tellus* 12:172–75
Stern ME. 1969. Collective instability of salt fingers. *J. Fluid Mech.* 35:209–18
Stern ME, Radko T, Simeonov J. 2001. Salt fingers in an unbounded thermocline. *J. Mar. Res.* 59:355–90
Stern ME, Simeonov JA. 2002. Internal wave overturns produced by salt fingers. *J. Phys. Oceanogr.* 32:3638–56
Stern ME, Turner JS. 1969. Salt fingers and convecting layers. *Deep Sea Res.* 16:97–511
Stevenson DJ. 1977. A semitheory for semiconvection. *Proc. Astron. Soc. Aust.* 3:165–66
Stevenson DJ. 1982. Formation of the giant planets. *Planet. Space Sci.* 30:755–64
Stevenson DJ. 1985. Cosmochemistry and structure of the giant planets and their satellites. *Icarus* 62:4–15
Stevenson DJ, Salpeter EE. 1977. The dynamics and helium distribution in hydrogen-helium fluid planets. *Astrophys. J. Supp. Ser.* 35:239–61

Stothers R, Chin CW. 1968. Evolution of massive helium-burning supergiants. *Astrophys. J.* 152:225–32
Stothers R, Simon NR. 1969. An explanation for the blue sequence of variable stars. *Astrophys. J.* 157:673–81
Straniero O, Domínguez I, Imbriani G, Piersanti L. 2003. The chemical composition of white dwarfs as a test of convective efficiency during core helium burning. *Astrophys. J.* 583:878–84
Sukhbold T, Woosley SE. 2014. The compactness of presupernova stellar cores. *Astrophys. J.* 783:10
Tait R, Howe M. 1968. Some observations of thermohaline stratification in the deep ocean. *Deep Sea Res.* 15:275–80
Tait R, Howe M. 1971. Thermohaline staircase. *Nature* 231:178–79
Timmermans ML, Toole J, Krishfield R, Winsor P. 2008. Ice-Tethered Profiler observations of the double-diffusive staircase in the Canada Basin thermocline. *J. Geophys. Res. Oceans* 113:C00A02
Traxler A, Garaud P, Stellmach S. 2011a. Numerically determined transport laws for fingering ("thermohaline") convection in astrophysics. *Astrophys. J. Lett.* 728:L29
Traxler A, Stellmach S, Garaud P, Radko T, Brummell N. 2011b. Dynamics of fingering convection. Part 1. Small-scale fluxes and large-scale instabilities. *J. Fluid Mech.* 677:530–53
Turner J. 1965. The coupled turbulent transports of salt and and heat across a sharp density interface. *Int. J. Heat Mass Transf.* 8:759–67
Turner J. 1974. Double-diffusive phenomena. *Annu. Rev. Fluid Mech.* 6:37–54
Turner J. 1985. Multicomponent convection. *Annu. Rev. Fluid Mech.* 17:11–44
Ulrich RK. 1972. Thermohaline convection in stellar interiors. *Astrophys. J.* 172:165–77
Vauclair S. 2004. Metallic fingers and metallicity excess in exoplanets' host stars: the accretion hypothesis revisited. *Astrophys. J.* 605:874–79
Veronis G. 1965. On finite amplitude instability in thermohaline convection. *J. Mar. Res.* 233:1–17
Walin G. 1964. Note on the stability of water stratified by both salt and heat. *Tellus* 16:389
Wood TS, Garaud P, Stellmach S. 2013. A new model for mixing by double-diffusive convection (semi-convection). II. The transport of heat and composition through layers. *Astrophys. J.* 768:157
Worster MG. 1997. Convection in mushy layers. *Annu. Rev. Fluid Mech.* 29:91–122
Wüest A, Sommer T, Carpenter JR. 2012. Diffusive-type of double diffusion in lakes—a review. In *Environmental Fluid Mechanics: Memorial Volume in Honour of Prof. Gerhard H. Jirka*, ed. W Rodi, M Uhlmann, pp. 271–84. Boca Raton, FL: CRC
Zaussinger F, Spruit HC. 2013. Semiconvection: numerical simulations. *Astron. Astrophys.* 554:A119

Annual Review of Fluid Mechanics

Volume 50, 2018

Contents

Indexes

Errata

An online log of corrections to *Annual Review of Fluid Mechanics* articles may be found at http://www.annualreviews.org/errata/fluid